JMEPEG (2012) 21:2295–2302
DOI: 10.1007/s11665-012-0185-4

1059-9495/$19.00

In Situ Production of Fe-TiC Nanocomposite by Mechanical Activation and Heat Treatment of the $Fe_2O_3/TiO_2/C$ Powder

Sara Moradi Ghiasabadi and Shahram Raygan

(Submitted May 8, 2011; in revised form February 1, 2012)

In this study, Fe-TiC nanocomposite was synthesized by carbothermic reduction of activated Fe_2O_3, TiO_2, and graphite powder mixture. The effect of 0, 5, and 20 h of high energy ball milling of mixture on the reduction process was also investigated. Comparing the results of the thermogravimetry analysis of milled and un-milled mixtures clearly showed that the reduction temperature decreased due to the milling process. XRD pattern of 20 h milled powder mixture proved that Fe-TiC nanocomposite was formed after the heat treatment of activated powder at 1100°C for 1 h under vacuum. The microstructure studies of the milled mixture by scanning electron microscope revealed homogenous distribution of TiC particles in the Fe matrix.

Keywords grinding, heat treating, metal matrix composite, powder metallurgy

1. Introduction

TiC is a good reinforcement in iron-based composites because of its high hardness, thermal stability, metallic properties, and resistance to abrasion wear (Ref 1-4). TiC particles can be produced through various ways such as welding (Ref 5, 6), ion beam sputtering (Ref 7), and aluminothermic and carbothermic reductions (Ref 8, 9). The in situ synthesized particles are more eligible to reinforce Fe matrix because they have smaller size and clean surface and they require cheaper initial materials (TiO_2 in comparison with Ti) (Ref 1-4). The mentioned methods present various characteristics of particle size and distribution, morphology of particles, state of agglomeration, and chemical purity. It has been reported that carbothermic reduction of titanium dioxide, TiO_2, occurs over the temperature range of 1700-2100 °C (Ref 10). Ilmenite has also been used as an initial material for this process. It has been proved that the milling powder mixture of carbon and TiO_2 or ilmenite decreases the time and temperature of the reduction process (Ref 11-14). Nanostructure TiC can be produced at ambient temperature by high energy milling using Ti and C as the initial materials. In addition, it has been reported that TiC cannot be produced by milling TiO_2 and carbon powder mixture because of its high positive formation free energy from these materials (Ref 12).

S. Moradi Ghiasabadi and **S. Raygan**, School of Metallurgy and Materials Engineering, College of Engineering, University of Tehran, Tehran 14399, Iran. Contact e-mails: saramgh@yahoo.com and shraygan@ut.ac.ir.

Mechanical milling of hematite and carbon powder mixture decreases the onset temperature of the reduction (Ref 15). This process can also change the rate of reduction at high temperature (Ref 13, 16-18). Cold welding and fracturing of powder particles during mechanical milling result in the decrease of the particle size and increase of the contact surface area between the reactants. Fine crystallite size, large special surface area (SSA), small particle size, less degree of long-range order, presence of internal strain and amorphous phases which are seen after mechanical activation lead to higher chemical reactivity. In addition, the rate of reaction and the controlling mechanism of overall rate will change by this process (Ref 13-15).

The aim of this study was to produce Fe-TiC nanocomposite by an in situ process using mechanical activation and heat treatment of Fe_2O_3-TiO_2-C powder mixture. The in situ technique involves a chemical reaction resulting in the formation of a very fine and stable ceramics phases within a metal matrix (Ref 19). The advantages of the in situ route are the clean surface of generated phase and homogenous distribution of the second phase in the matrix. In this situation, the matrix-reinforcement interface bonds tend to be stronger (Ref 1, 3, 19, 20).

2. Experimental Procedures

In this study, powder of anatase (>99% TiO_2, particle size ≤ 5 μm), graphite (>99% carbon, particle size 5-10 μm) and hematite (>99% Fe_2O_3, particle size ≤ 5 μm) was used as starting materials. Stoichiometric ratio of iron and titanium oxides with 10 mol% of excess graphite was mixed in order to produce Fe-15 wt.%TiC composite. Milling was carried out in the Fritsch P6 high energy planetary ball mill using balls of 10 and 20 mm diameter and ball to powder mass ratio of 20. The rotation speed of vials was 300 rpm and milling was continued up to 20 h under argon atmosphere. Scanning electron microscope

(SEM) (camscan MV2300 in Backscatter mode (BS)) was employed to study the morphology of milled and un-milled powder. 0.05 g of un-milled and 5 and 20 h milled samples were heated to 1100 °C at the rate of 10 °C/min in the flowing argon atmosphere in a TGA (thermogravimetric analyzer Netzsch STA 409). The RTG curve (rate of mass change) was calculated from TGA data as follows:

$$\mathrm{RTG}\ (\%/\mathrm{s}) = -\frac{d(\mathrm{TG})}{dt} \times 100 \qquad \text{(Eq 1)}$$

According to the results of the TGA experiments, the remained powder was pressed and heat treated under the vacuum at different constant temperatures for 60 min.

The phases in the samples were characterized by Philips Xpert, X-ray diffractometer (XRD) at 40 kV and 100 mA with the Co Kα radiation.

3. Result and Discussion

The XRD patterns of the un-milled and milled samples are shown in Fig. 1. Hematite (Fe_2O_3), anatase (TiO_2), and graphite phases were seen in the pattern of the un-milled sample. The graphite could not be detected in the XRD patterns of the 5 h milled sample because of amorphization of this phase during the milling process. This phenomenon was also reported in other studies (Ref 15-18). The hematite structure remained stable during the continued milling up to 20 h. The most intense peak of anatase was not detected after 10 h while other peaks of anatase disappeared after 5 h of milling, probably due to the amorphization of anatase. In addition, new phases could not be observed in the XRD pattern of the milled powder, suggesting that no significant chemical reduction took place during the entire milling process. The decrease in the integral intensity of hematite peaks and broadening of its peaks during the milling process indicated the reduction of the size of the hematite crystallites and the presence of the internal strain.

The crystallite size of hematite in the milled mixtures was estimated by Williamson-Hall equation (Eq. 2). Table 1 demonstrates the results, after modifying the instrument broadening (Ref 21).

$$\beta \cos\theta = \frac{k\lambda}{d} + 2\varepsilon \sin\theta \qquad \text{(Eq 2)}$$

In this equation, β is full width at half maximum, k is Scherer's constant (usually equal to 0.9), D is crystal diameter, ε is internal stress, and λ is wave length of X-ray. The crystallite size of hematite was reduced gradually during the milling time and reached 18 nm after 20 h of milling while internal strain increased. Accordingly, high fraction of the boundary regions existed between nanocrystallites of hematite. These boundaries had a highly disordered structure which increased reactivity of the powder mixture. The backscatter SEM images of the un-milled and milled powder mixtures are shown in Fig. 2.

Figure 2(a) and (b) shows the black flakes of graphite in the un-milled powder. White particles of hematite and grey particles of anatase in a spherical shape were obvious at higher magnification according to their atomic weight (Fig. 2b). Figure 2(c) shows that, after 2 h of milling, the milled mixture consisted of both tiny individual particles and large agglomerates of small particles. The shape, size, and quantity of agglomerates changed with the increase in the milling time. The shape of agglomerates partially changed from semi-round (Fig. 2c) to flat (Fig. 2d) after 5 h of milling. The size of large flat agglomerates decreased after 10 h of milling (Fig. 2e). Increasing the milling time up to 20 h decreased the quantity of large agglomerates (Fig. 2f).

Figure 3 shows the morphology of individual particles and agglomerates in the milled mixtures. Figure 3(a) demonstrates that after 5 h of milling, agglomerates mainly consisted of gray and black particles. According to their atomic weight in backscatter images, it seems that these particles were anatase and graphite, respectively. Individual particles after 5 h of milling mainly consisted of white particles (Fig. 3b). After 10 h

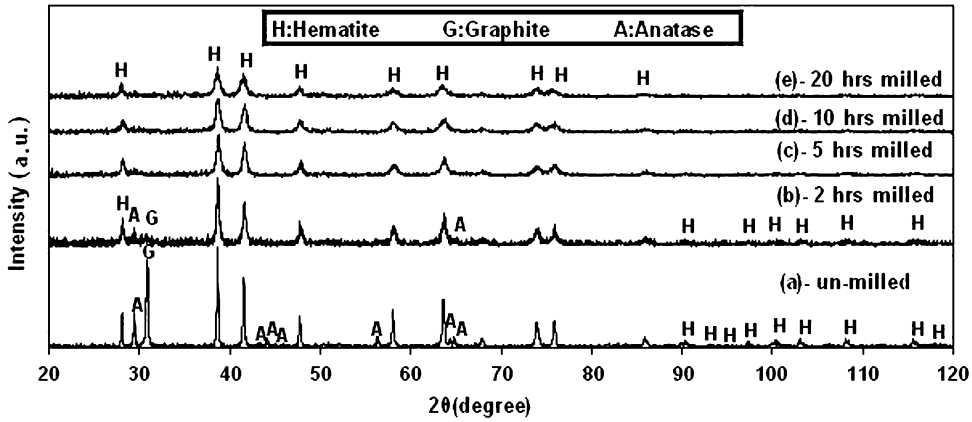

Fig. 1 XRD patterns of un-milled and milled Fe_2O_3, TiO_2, and graphite powder mixture

Table 1 Crystallite size of hematite before and after milling

Milling time (h)	0	2	5	10	20
Hematite crystallite size (nm)	60	62	38	23	18
Internal strain (%)	0.001	0.002	0.004	0.004	0.004

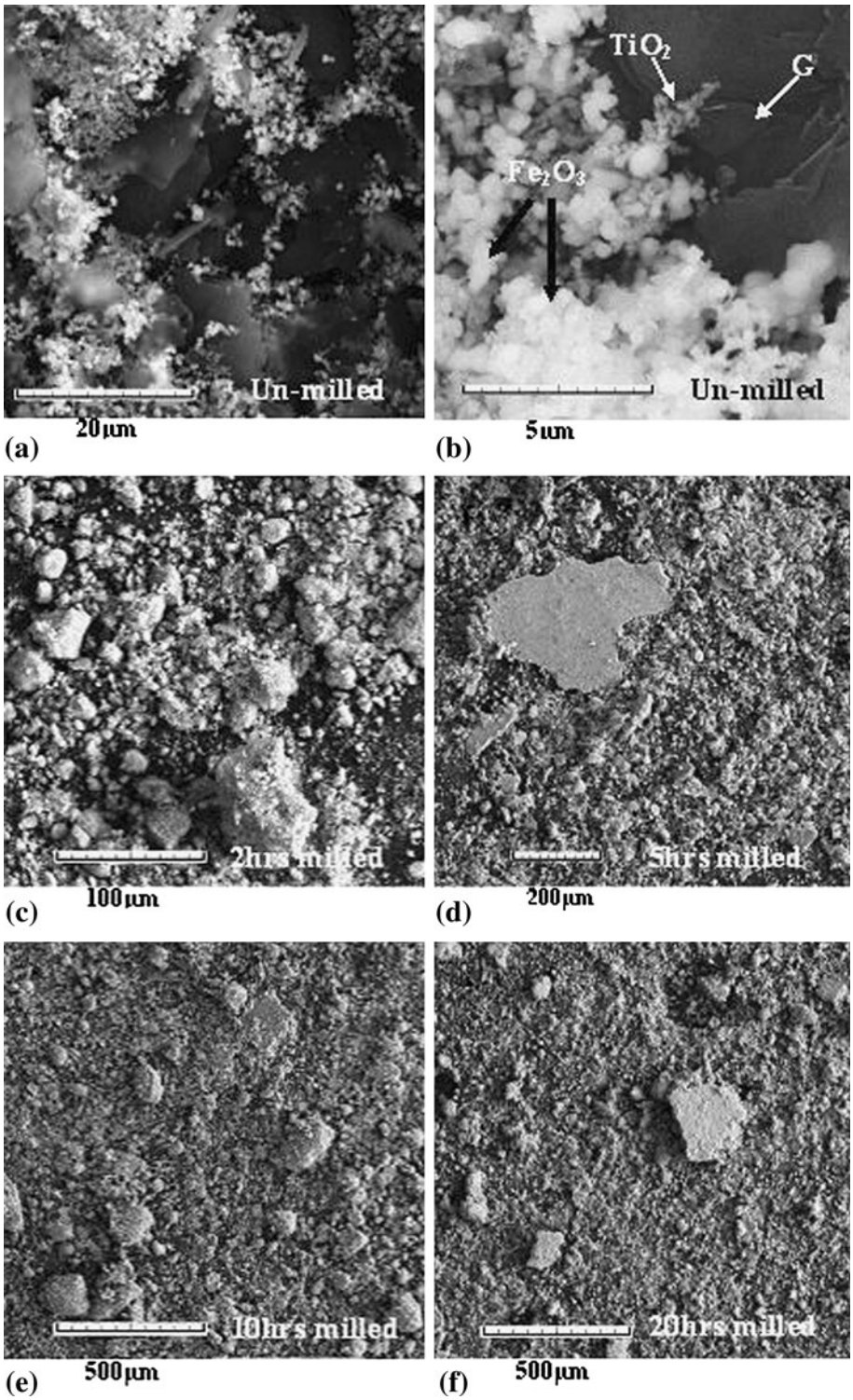

Fig. 2 The morphology of (a, b) un-milled, (c) 2 h, (d) 5 h, (e) 10 h, (f) 20 h milled powder mixture

of milling, white and grey particles could be observed in both agglomerates and individual particles of Fig. 3(c) and (d), respectively, while there was not any significant difference between the composition of agglomerates and individual particles after 20 h of milling (Fig. 3e and f).

These results showed that, at the beginning of milling, gray (anatase) and black (graphite) particles agglomerated. After 5 h of milling, the agglomerates broke down to smaller particles and, subsequently, these particles mixed together. Homogenous powder mixture was formed after 20 h of milling.

Figure 4 shows the results of TGA experiments of un-milled and milled powder mixtures. The increased reactivity from mechanical activation was confirmed by comparing the results of the TG tests on un-milled and milled mixtures where the temperature of reaction decreased in accordance with the milling time. The mass loss up to 800 °C for un-milled powder (Fig. 4a) which was the onset of the

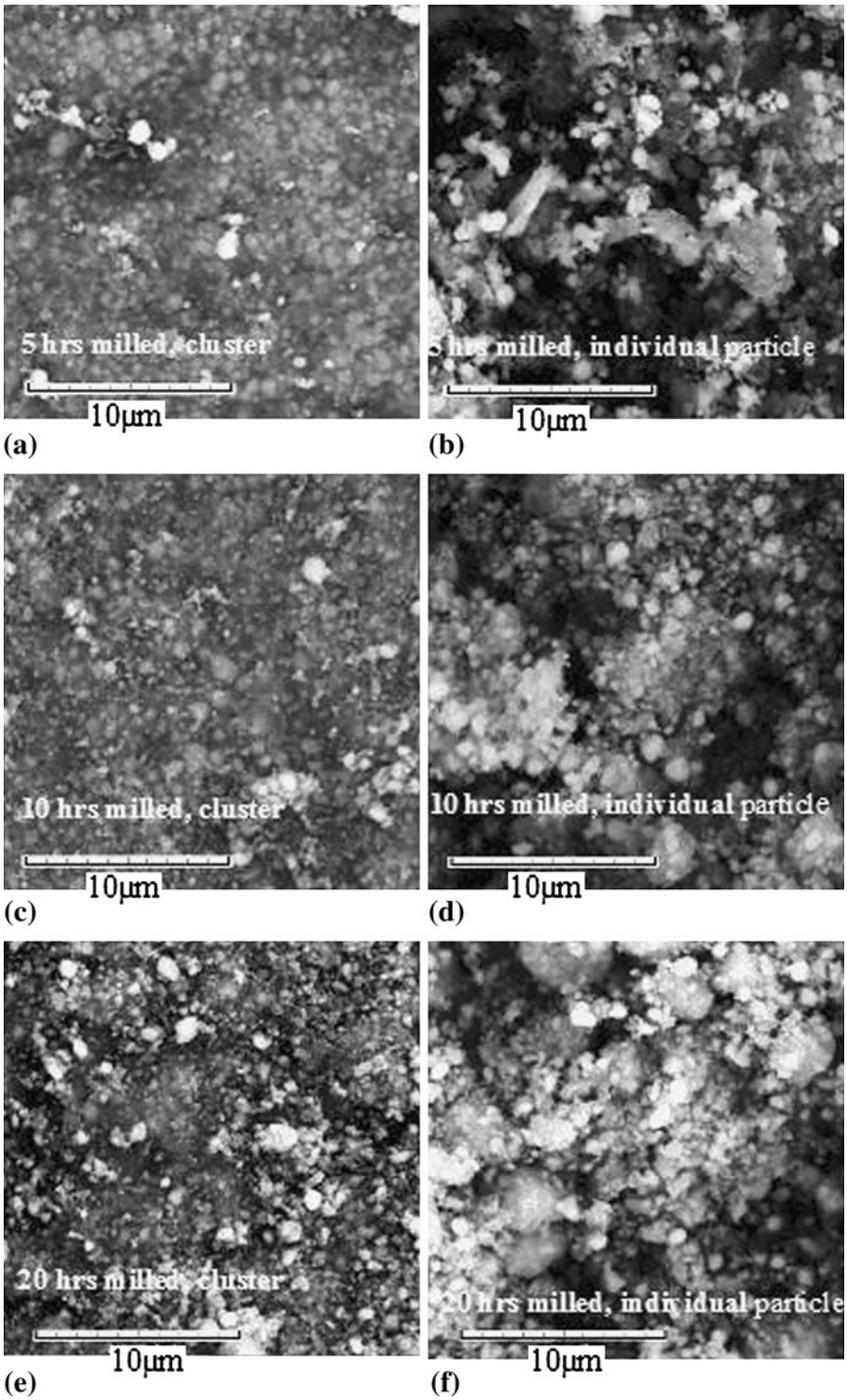

Fig. 3 Morphology of matrix and agglomerates in the milled powders for (a) 5 h particles, (b) 5 h agglomerates, (c) 10 h particles, (d) 10 h agglomerates, (e) 20 h particles, (f) 20 h agglomerates

first peak in the RTG curve was related to the adsorbed gases and moisture on the surface of the powder. This point appeared at 580 and 500 °C for 5 and 20 h of milling, respectively.

The mass loss for 0, 5, and 20 h of milling up to the mentioned temperature was 2.26, 3.54, and 4.08%, respectively. These mass losses showed increased amounts of adsorbed gases and moisture in accordance with the milling time due to the increase of the specific surfaces. The second peak of RTG curves was related to the reduction of hematite to magnetite according to Eq 3. The mass loss of this state (H $\rightarrow$ M) was about 3% for all the samples which was close to the theoretical mass loss (Ref 22-24).

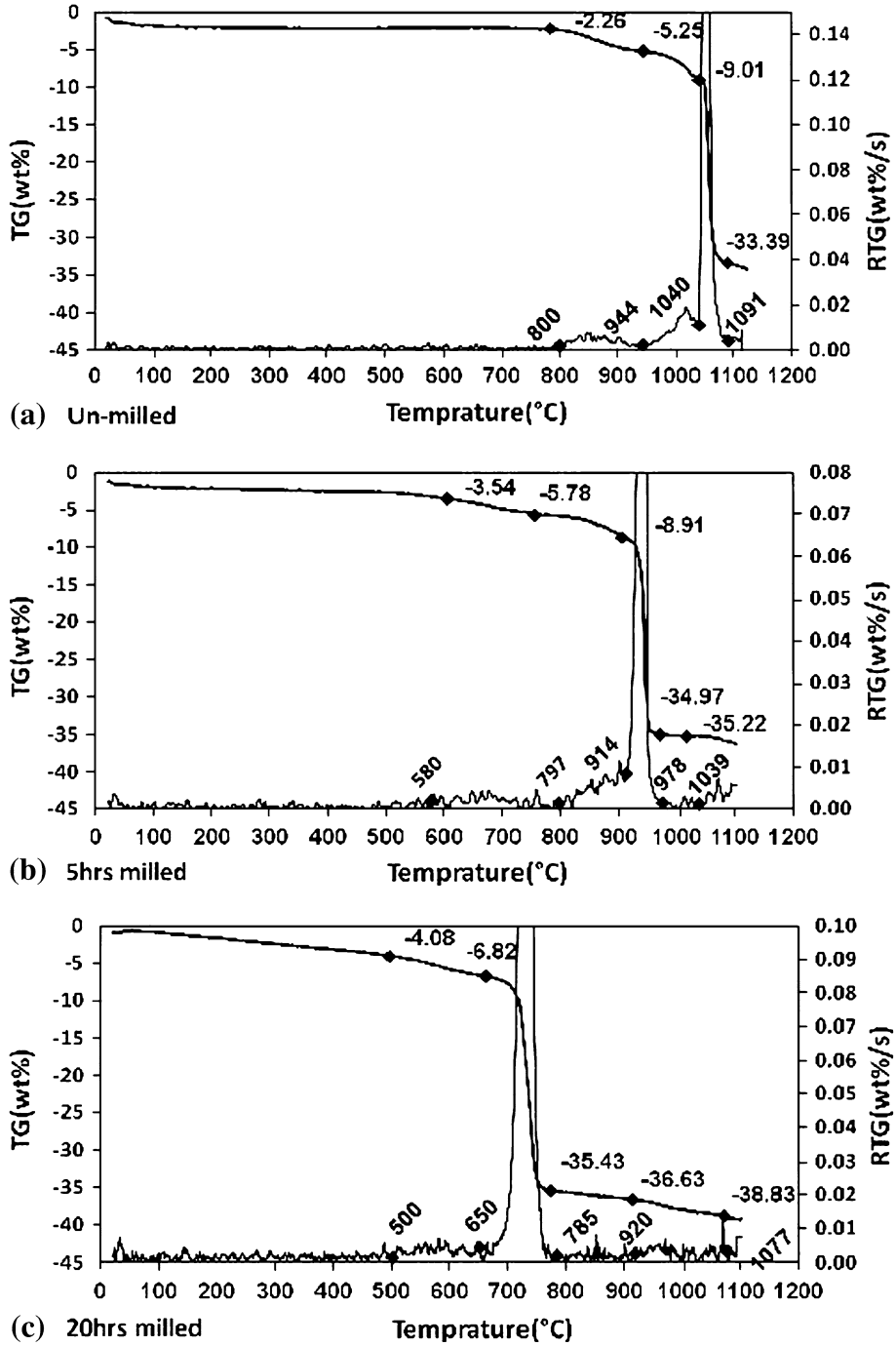

Fig. 4 TG-RTG curves of (a) 0, (b) 5, (c) 20 h milled samples

$$3Fe_2O_3 + 9C \rightarrow 2Fe_3O_4 + CO + 8C \quad \Delta W\% = 3.9 \qquad \text{(Eq 3)}$$

It has been reported that the reduction of Fe_2O_3 with C is not a simple reaction and goes through several stages (Ref 18-24). There is not any report on the formation of Fe_3C in these stages. The results of this study also did not show any trace of iron carbide which was in agreement with the above mentioned mechanism.

The next peak in the RTG curves was related to the overlapping reductions of magnetite to wustite (M → W) and wustite to iron (W → Fe). The starting point of these stages for the un-milled sample was 944 °C which decreased to 798 and 650 °C for 5 and 20 h of milling, respectively. The RTG curve for un-milled sample indicated that the formation of iron began before the completion of magnetite to wustite stage. The mass loss of this stage was about 3% which was lower than that of the theoretical value (Eq 4) (Ref 22-24). It can be concluded that the stages of M → W and W → Fe were overlapping, which was in agreement with the findings of others (Ref 15-18).

$$2Fe_3O_4 + 8C \rightarrow 6FeO + 2CO + 6C \quad \Delta W\% = 7.8 \qquad \text{(Eq 4)}$$

Formation of iron was completed at 1090 °C for the un-milled sample but this temperature decreased to 978 and

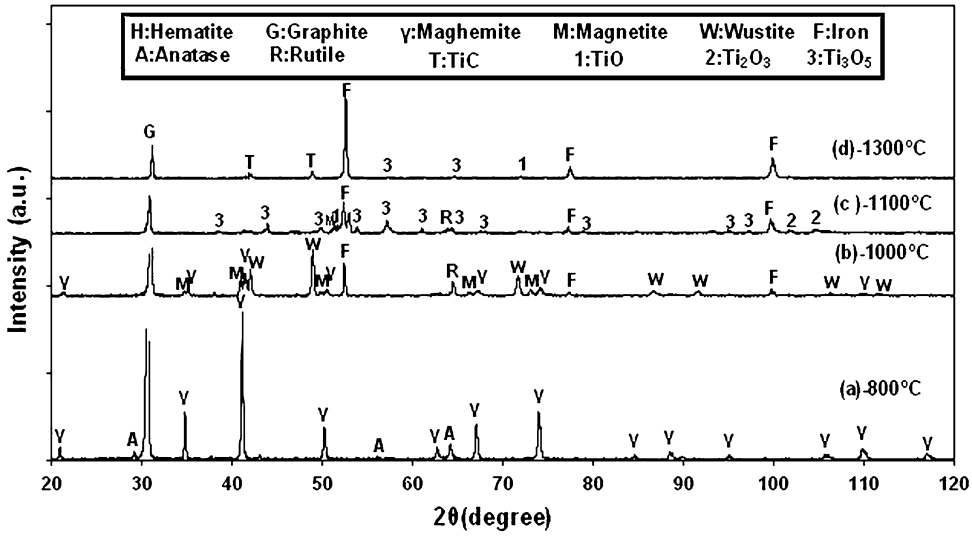

Fig. 5 XRD patterns of un-milled powder mixture after heating to (a) 800 °C, (b)1000 °C, (c) 1100 °C, (d)1300 °C

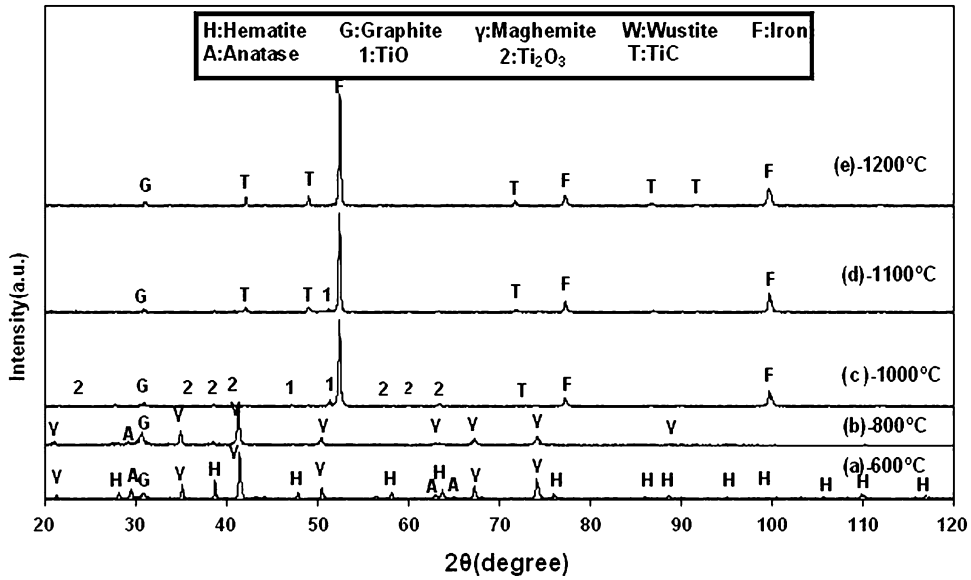

Fig. 6 XRD patterns of 5 h milled powder mixture after heating to (a) 600 °C, (b) 800 °C, (c) 1000 °C, (d) 1100 °C, (e) 1200 °C

785 °C for 5 and 20 h of the milled samples, respectively. The mass loss of samples up to the end of the last peak (main peak) was 31.3% which was close to the theoretical mass loss according to Eq 5.

$$3Fe_2O_3 + 9C \rightarrow 6Fe + 9CO \quad \Delta W\% = 35.1 \qquad \text{(Eq 5)}$$

It has been reported that carbothermic reduction of TiO_2 starts at temperatures higher than 1100 °C (Ref 12). Therefore, mass loss due to the reduction of TiO_2 cannot be seen in the TG curve of un-milled sample. However, mass loss after the end of Fe formation in the TG curves demonstrated traces of carbothermic reduction of TiO_2 in 5 and 20 h milled powders after the formation of iron.

The XRD patterns of un-milled samples after heating to 800, 1000, 1100, and 1300 °C are shown in Fig. 5. The peaks of C, TiO_2, and γ-Fe_2O_3 phases can be seen in the pattern of the powder heated to 800 °C. The peaks of γ-Fe_2O_3, Fe_3O_4, FeO, and Fe phases appeared in the powder heated to 1000 °C due to the sequential reduction of iron oxide. It should be noted that identification of the Ti_nO_{2n-1} phases (titanium sub-oxides) where $n \geq 3$ is difficult. These phases have very similar XRD patterns and the intensity of distinguishing peaks is low (Ref 2, 10, 20). At 1000 °C, the most intense peak of the rutile became visible. Rutile is more stable than anatase. Thus, anatase can be transformed into rutile during heating or ball milling (Ref 10). The increase in the temperature to 1100 °C led to the complete reduction of iron oxide and appearance of TiO, Ti_3O_5, and Ti_2O_3 phases. At 1300 °C, in addition to TiO and Ti_3O_5 phases, the peaks of TiC also appeared. Therefore, it can be concluded that the synthesis of Fe-TiC composite was not completed up to 1300 °C in un-milled powder mixture. The increase of the intensity of iron peaks at the temperature of 1300 °C indicated the partial recrystallisation of this phase.

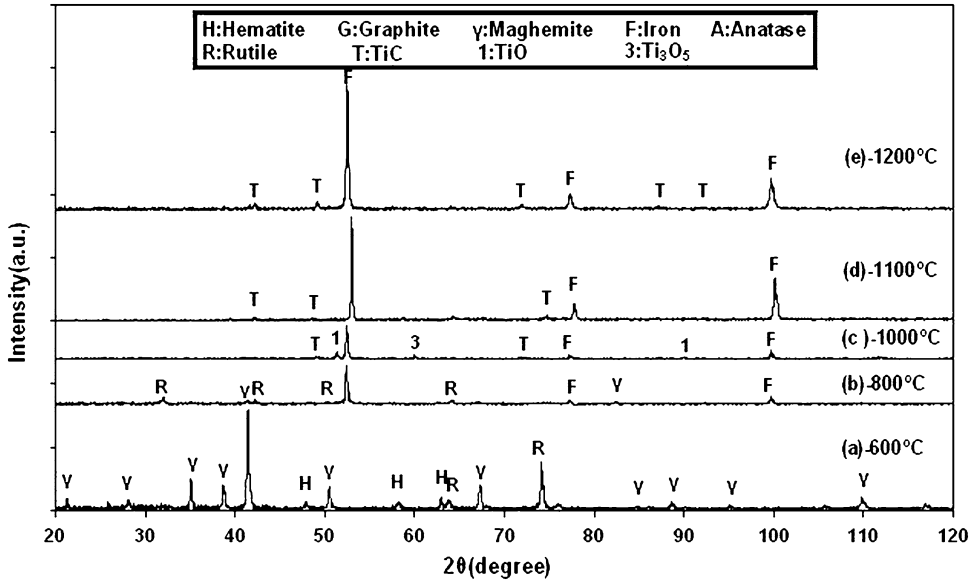

Fig. 7 XRD patterns of 20 h milled powder mixture after heating to (a) 600 °C, (b) 800 °C, (c) 1000 °C, (d) 1100 °C, (e) 1200 °C

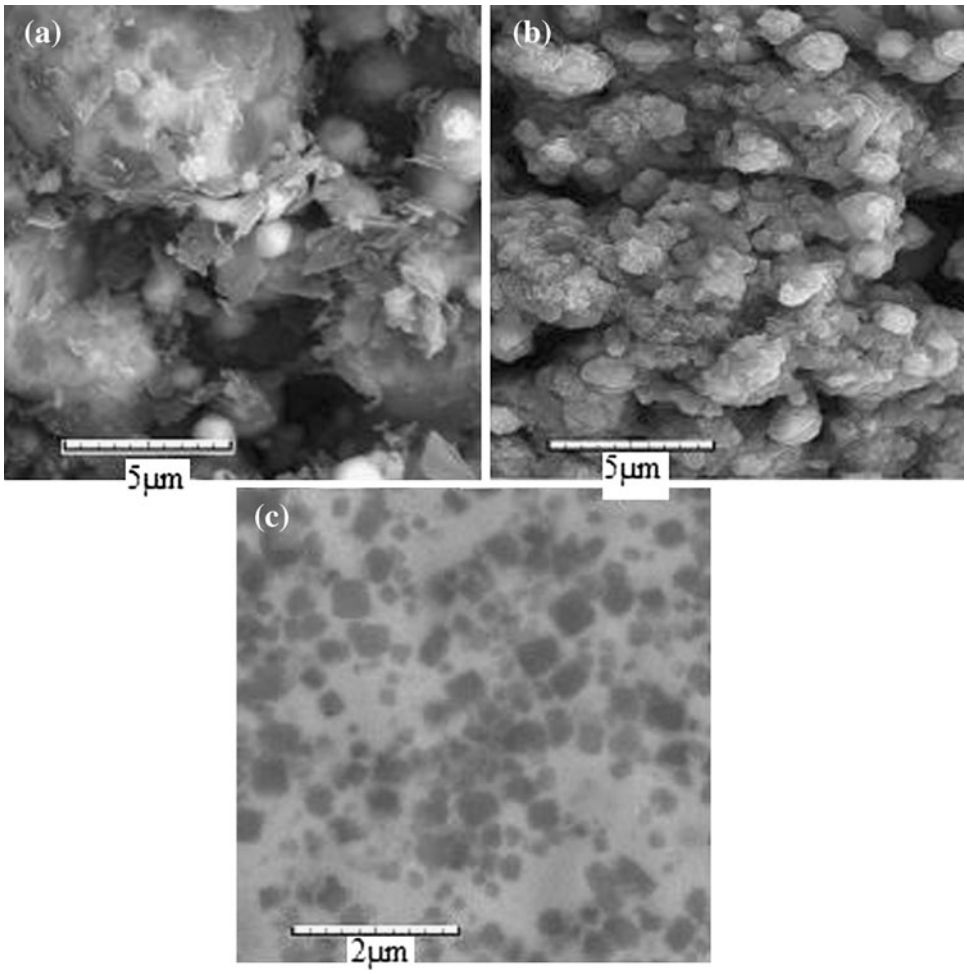

Fig. 8 SEM images of Fe-TiC composite at (a) heating the 5 h milled powder to 1200 °C, (b) heating the 20 h milled powder to 1100 °C, (c) heating the 20 h milled powder to 1200 °C

Figure 6 shows XRD patterns of 5 h milled powder mixture after heating to 600, 800, 1000, 1100, and 1200 °C. Anatase, graphite, maghemite, and hematite phases can be observed in the patterns of powder heated to 600 °C. Existence of maghemite with hematite indicated the initiation of hematite reduction. Further heating to 800 °C led to the completion of maghemite formation. The main peak of anatase was remained at this temperature indicating that transformation of anatase was not completed in this condition.

Reduction of iron oxide to iron was completed and titanium oxides were reduced to Ti_2O_3 and TiO at temperature of 1000 °C. The increase of temperature to 1100 °C led to partial formation of TiC from titanium oxide. At the temperature of 1200 °C, the complete synthesis of Fe-TiC composite occurred. The crystallite size of iron which was 39 nm at 1000 °C increased to 43 nm at 1200 °C. It can be concluded from Fig. 5 and 6 that the onset temperature of TiO_2 reduction and final temperature of iron formation decreased after 5 h of milling. Synthesis of Fe-TiC composite was completed after 5 h of pre-milling and subsequent heating to 1200 °C. The crystallite size of iron and TiC in the composite was 47 and 42 nm, respectively.

Figure 7 shows XRD patterns of 20 h milled powder mixture after being heated to 600, 800, 1000, and 1100 °C. It can be seen that the temperature of transformation of anatase to rutile decreased to 600 °C after 20 h of pre-milling due to the accumulation of energy in the powder. Synthesis of iron was completed at 800 °C. Ti_3O_5, TiO, and main peak of TiC could be observed at the temperature of 1000 °C. The Fe-TiC composite was formed at 1100 °C with the crystallite size of 51 nm for iron and 39 nm for TiC.

The SEM images of Fe-TiC composites were synthesized due to heating of 5 h milled powder at 1200 °C and 20 h milled powder at 1200 °C, as shown in Fig. 8.

The purpose of this research was to synthesize Fe-TiC composite. The composite was formed at 1200 °C after 5 h of pre-milling and at 1100 and 1200 °C after 20 h of pre-milling. The bulk composite of iron with dispersed TiC was formed at the temperature of 1200 °C for 20 h milled powder probably due to the sintering of the particles.

4. Conclusions

In this study, the reduction behaviors of milled TiO_2, Fe_2O_3, and C were investigated. The results could be summarized as follows:

- Carbothermic reduction in the powder mixture could not be observed during milling.
- The TG curves showed that the reduction temperature decreased significantly with the increase in the milling time.
- Nanocrystalline Fe and TiC powder composite was produced by heating 5 and 20 h milled mixture at 1200 and 1100 °C, respectively.
- Nanocrystalline Fe and TiC bulk composite was formed by heating 20 h milled mixture to 1200 °C.

References

1. Y. Wang, X. Zhang, F. Li, and G. Zeng, Study on an Fe-TiC Surface Composite Produced In Situ, *Mater Des*, 1999, **20**, p 233–236
2. N. Setoudeh, A. Saidi, and N.J. Welham, Effect of Elemental Iron and Gas Atmosphere on the Carbothermic Reduction of Rutile, *J. Alloys Compd.*, 2006, **419**, p 247–250
3. N.J. Welham and J.S. Wiliams, Carbothermic Reduction of Ilmenite and Rutile, *Metall. Mater. Trans.*, 1999, **30B**, p 1075–1081
4. H. Jia, Z. Zang, Z. Qi, G. Liu, and X. Bian, Formation of Nanocrystalline TiC from Titanium and Different Carbon Sources by Mechanical Alloying, *J. Alloys Compd.*, 2009, **472**(1–2), p 97–103
5. X.H. Wang, M. Zhang, Z.D. Zou, S.L. Song, F. Han, and S.Y. Qu, In Situ Production of Fe-TiC Surface Composite Coatings by Tungsten-Inert Gas Heat Source, *Surf. Coat. Technol.*, 2006, **200**, p 6117–6122
6. X.H. Wang, S.L. Song, S.Y. Qu, and Z.D. Zou, Characterization of In Situ Synthesized TiC Particle Reinforced Fe-based Composite Coatings Produced by Multi-Pass Overlapping GTAW Melting Process, *Surf. Coat. Technol.*, 2007, **201**, p 5899–5905
7. J. Wang, W.Z. Li, and H.D. Li, Mechanical Properties of Nanoscaled TiC-Fe Multilayers Deposited by Ion Beam Sputtering Technique, *Thin Solid Films*, 2001, **382**, p 190–193
8. K. Das and T.K. Bandyopadhyay, Effect of Form of Carbon on the Microstructure of In Situ Synthesized TiC-reinforced Iron-based Composite, *Mater. Lett.*, 2004, **58**, p 1877–1880
9. Z. Mei, Y.W. Yan, and K. Cui, Effect of Matrix Composition on tMicrostructure of In-Situ Synthesized TiC Particulate Reinforced Iron-based Composites, *Mater. Lett.*, 2003, **57**, p 3175–3181
10. N. Setoudeh, A. Saidi, and N.J. Welham, Carbothermic Reduction of Anatase and Rutile, *J. Alloys Compd.*, 2005, **390**, p 138–143
11. A. Calka, D. Oleszak, and N. Stanford, Rapid Synthesis of TiC-Fe_3C Composite by Electric Discharge Assisted Mechanical Milling of Ilmenite with Graphite, *J. Alloys Compd.*, 2008, **459**, p 498–500
12. R.M. Ren, Z.G. Yang, and L.L. Shaw, Synthesis of Nanostructured TiC via Carbothermic Reduction Enhanced by Mechanical Activation, *Scripta Mater.*, 1998, **38**, p 735–741
13. Y. Kashiwaya, H. Suzuki, and K. Ishii, Gas Evolution During Mechanical Milling of Hematite-Graphite Mixture, *ISIJ Int.*, 2004, **l44**, p 1970–1974
14. P. Pourghahramani and E. Forssberg, Effect of Mechanical Activation on the Reduction Behavior of Hematite Concentrate, *Int. J. Miner. Process.*, 2007, **82**, p 96–105
15. S. Raygan, J.V. Khaki, and M.R. Aboutalebi, The Effect of Mechanical Milling on the Carbothermic Reduction of Hematite, *Miner. Process. Extr. Metall. Rev.*, 2003, **24**, p 1–19
16. S. Raygan, J.V. Khaki, and M.R. Aboutalebi, Effect of Mechanical Activation on the Packed-Bed, High-Temperature Behavior of Hematite and Graphite Mixture in Air, *J. Mater. Synth. Process.*, 2002, **10**, p 113–120
17. J.V. Khaki, Y. Kashiwaya, K. Ishii, and H. Suzuki, Intensive Improvement of Reduction Rate of Hematite-Graphite Mixture by Mechanical Milling, *ISIJ Int.*, 2002, **142**, p 13–22
18. Y. Kashiwaya, H. Suzuki, and K. Ishii, Characteristics of Nano-reactor and Phenomena During Mechanical Milling of Hematite-Graphite Mixture, *ISIJ Int.*, 2004, **44**, p 1975–1980
19. W. Jing and W. Yisan, In-situ Production of Fe-TiC Composite, *Mater. Lett.*, 2007, **61**, p 4393–4395
20. C. Fengjun and W. Yisan, Microstructure of Fe-TiC Surface Composite Produced by Cast-Sintering, *Mater. Lett.*, 2007, **61**, p 1517–1521
21. B.D. Cullity, *Elements of X-ray Diffraction*, Addison-Wesly, Reading, MA, 1978
22. K.I. Otsuka and O. Kuni, Reduction of Powdery Ferric Oxide Mixed with Graphite Particles, *J. Chem. Eng. Jpn.*, 1969, **2**, p 46–50
23. F. Ajersch, Chemical and Physical Characteristics Affecting the Reduction Kinetics of Iron Oxide Pellets with Solid Carbon, *Can. Metall. Q.*, 1988, **27**, p 137–143
24. S.H. Huang and W.-K. Lu, Kinetics and Mechanisms of Reaction in Iron Ore/Coal Composites, *ISIJ Int.*, 1993, **33**, p 1055–1061